THE JOURNAL OF BIOLOGICAL CHEMISTRY VOL. 282, NO. 17, pp. 12755–12764, April 27, 2007

Molecular Basis of the Isoform-specific Ligand-binding Affinity of Inositol 1,4,5-Trisphosphate Receptors*[S]

Received for publication, October 18, 2006, and in revised form, February 1, 2007 Published, JBC Papers in Press, February 27, 2007, DOI 10.1074/jbc.M609833200

Miwako Iwai[‡], Takayuki Michikawa[‡§¶1], Ivan Bosanac[‖], Mitsuhiko Ikura[‖], and Katsuhiko Mikoshiba[‡§¶2]

From the [‡]Division of Molecular Neurobiology, Department of Basic Medical Sciences, Institute of Medical Science, University of Tokyo, 4-6-1 Shirokanedai, Minato-ku, Tokyo 108-8639, Japan, the [§]Laboratory for Developmental Neurobiology, Brain Science Institute, RIKEN, Saitama 351-0198, Japan, the [¶]Calcium Oscillation Project, International Cooperative Research Project-Solution Oriented Research for Science and Technology, Japan Science and Technology Agency, Saitama 332-0012, Japan, and the [‖]Division of Signaling Biology, Ontario Cancer Institute, Department of Medical Biophysics, University of Toronto, Toronto, Ontario M5G 1L7, Canada

Three isoforms of the inositol 1,4,5-trisphosphate (IP_3) receptor (IP_3R), IP_3R1, IP_3R2, and IP_3R3, have different IP_3-binding affinities and cooperativities. Here we report that the amino-terminal 604 residues of three mouse IP_3R types exhibited K_d values of 49.5 ± 10.5, 14.0 ± 3.5, and 163.0 ± 44.4 nM, which are close to the intrinsic IP_3-binding affinity previously estimated from the analysis of full-length IP_3Rs. In contrast, residues 224–604 of IP_3R1 and IP_3R2 and residues 225–604 of IP_3R3, which contain the IP_3-binding core domain but not the suppressor domain, displayed an almost identical IP_3-binding affinity with a K_d value of ~2 nM. Addition of 100-fold excess of the suppressor domain did not alter the IP_3-binding affinity of the IP_3-binding core domain. Artificial chimeric proteins in which the suppressor domain was fused to the IP_3-binding core domain from different isoforms exhibited IP_3-binding affinity significantly different from those of the proteins composed of the native combination of the suppressor domain and the IP_3-binding core domain. Systematic mutagenesis analyses showed that amino acid residues critical for type-3 receptor-specific IP_3-binding affinity are involved in Glu-39, Ala-41, Asp-46, Met-127, Ala-154, Thr-155, Leu-162, Trp-168, Asn-173, Asn-176, and Val-179. These results indicate that the IP_3-binding affinity of IP_3Rs is specifically tuned through the intramolecular attenuation of IP_3-binding affinity of the IP_3-binding core domain by the amino-terminal suppressor domain. Moreover, the functional diversity in ligand sensitivity among IP_3R isoforms originates from at least the structural difference identified on the suppressor domain.

The inositol 1,4,5-trisphosphate (IP_3)[3] receptors (IP_3Rs) function as IP_3-gated Ca^{2+} release channels located on intracellular Ca^{2+} stores, such as the endoplasmic reticulum (1). Mammalian IP_3R family consists of three isoforms (IP_3R1, IP_3R2, and IP_3R3), and they form homotetrameric or heterotetrameric channels (2). There is evidence of a functional difference among the three isoforms of IP_3R in terms of their IP_3 sensitivity (3–5) and cooperativity with respect to IP_3 binding (5). The intrinsic association constants of mouse IP_3R1, IP_3R2, and IP_3R3 expressed in Sf9 cells are estimated to be 3.5×10^7, 1.7×10^8, and 3.4×10^6 (M^{-1}), respectively (5). IP_3R2 exhibits both negative and positive cooperativity, whereas IP_3R3 exhibits negative IP_3 binding cooperativity (5). This diversity of responsiveness to IP_3 observed among the three IP_3R isoforms may contribute to the generation of the different degree of IP_3 sensitivity of the Ca^{2+} store. The molecular basis of the isoform-specific IP_3-binding affinity, however, is not well understood.

The IP_3-binding domain of IP_3R1 is composed of two functional domains, the amino-terminal suppressor domain and the carboxyl-terminal IP_3-binding core domain (6). The IP_3-binding core domain is the minimum region required for specific IP_3 binding and is mapped within residues 226–578 of mouse IP_3R1, a polypeptide of 2749 residues (6). The amino-terminal 225 amino acid residues of IP_3R1 function as the suppressor for IP_3 binding, and deletion of these residues results in significant enhancement of IP_3 binding (6). The atomic resolution structures of both the suppressor domain (7) and the IP_3-binding core domain (8) of mouse IP_3R1 were solved by x-ray crystallography to 1.8- and 2.2-Å resolution, respectively. The IP_3-binding core domain comprises two asymmetric domains, the β-domain and α-domain. A highly positive-charged pocket is created at the interface of these two domains to which an IP_3 molecule binds. The 11 amino acid residues in the IP_3-binding core domain of IP_3R1 are responsible for the coordination of IP_3 (8), and all of them except Gly-268 are conserved in other isoforms. The suppressor domain contains a β-trefoil fold and a helix-turn-helix structure inserted between two β-strands of the β-trefoil fold (7). The conserved 7 amino acid residues, which are clustered on one side of the suppressor domain, were found to be critical for the suppression of IP_3 binding (7). These structural and functional analyses of the IP_3-binding domain have been carried out mainly using the type-1 isoform, and the suppression ability of the amino-terminal regions of IP_3R2 and IP_3R3 has not been well characterized.

* This work was supported by the Ministry of Education, Culture, Sports, Science and Technology of Japan (Grants 17017013 and 17570128 to T. M. and Grant 15100006 to K. M.), by the Heart and Stroke Foundation of Canada (to M. I.), and by the Moritani Scholarship Foundation (to T. M.). The costs of publication of this article were defrayed in part by the payment of page charges. This article must therefore be hereby marked "*advertisement*" in accordance with 18 U.S.C. Section 1734 solely to indicate this fact.

[S] The on-line version of this article (available at http://www.jbc.org) contains supplemental Tables S1–S3, Figs. S1–S3, and an additional reference.

[1] To whom correspondence may be addressed. Tel.: 81-3-5449-5317; Fax: 81-3-5449-5420; E-mail: takamich@ims.u-tokyo.ac.jp.

[2] To whom correspondence may be addressed. Tel.: 81-3-5449-5316; Fax: 81-3-5449-5420; E-mail: mikosiba@ims.u-tokyo.ac.jp.

[3] The abbreviations used are: IP_3, inositol 1,4,5-trisphosphate; IP_3R, IP_3 receptor.

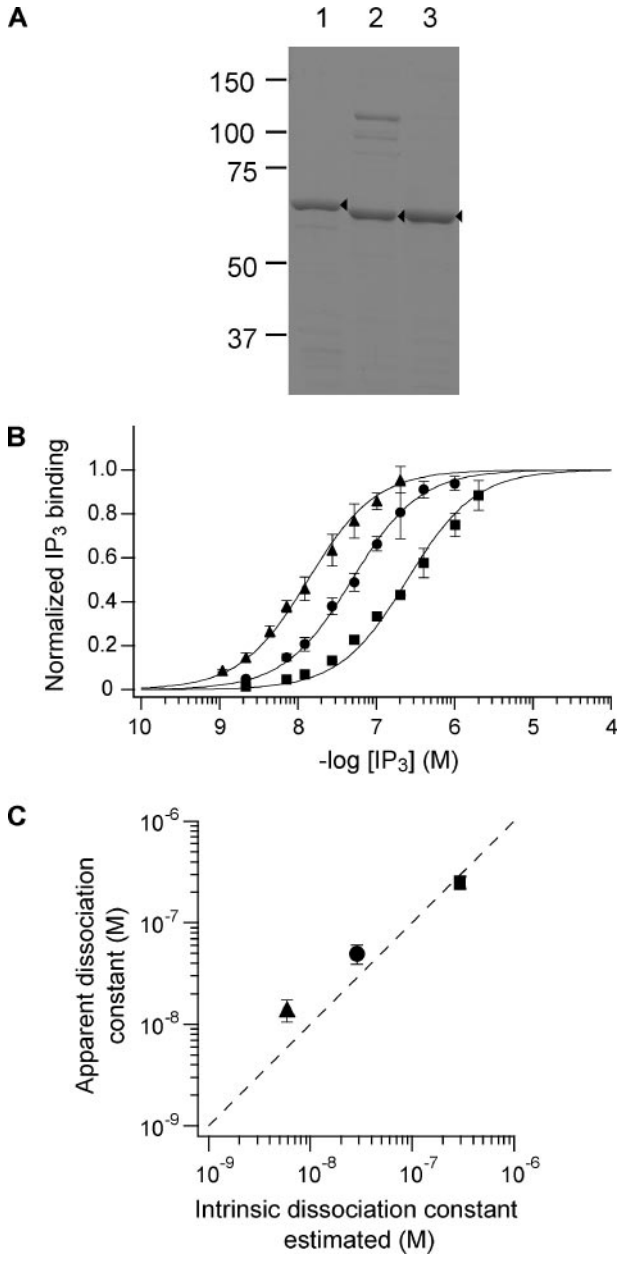

FIGURE 1. **Comparison of IP_3-binding affinity of the amino-terminal 604 residues among the three IP_3R isoforms.** *A*, SDS-PAGE analysis of T604s. Purified proteins (1 μg each) of $T604_{m1}$ (*lane 1*), $T604_{m2}$ (*lane 2*), and $T604_{m3}$ (*lane 3*) were separated on 7.5% SDS-PAGE followed by Coomassie Brilliant Blue R-250 staining. *Arrowheads* indicate T604 proteins. Molecular size makers are shown on the *left* ($\times 10^3$). *B*, equilibrium IP_3-binding activity of the IP_3-binding domains of the three IP_3R isoforms. Values are averages of 3 ($T604_{m1}$, *circle*), 3 ($T604_{m2}$, *triangle*), and 9 ($T604_{m3}$, *square*) measurements. *Error bars* correspond to the standard deviation. *C*, comparison between the apparent dissociation constants of T604 and the intrinsic dissociation constants estimated from the measurements using full-length IP_3Rs expressed in Sf9 cells (5). *Circle*, IP_3R1; *triangle*, IP_3R2; and *square*, IP_3R3. *Error bars* correspond to the standard deviation.

In the present study, we analyzed the IP_3-binding affinity of the IP_3-binding domain of three isoforms and found that the intramolecular suppression of IP_3 binding specifically tunes the IP_3-binding affinity of IP_3R isoforms. Systematic analyses of chimeric mutants and site-directed mutants created based on the three-dimensional structures of the suppressor domain provide us with a novel insight into the structural basis of the isoform-specific IP_3-binding affinity of the three IP_3R types.

EXPERIMENTAL PROCEDURES

Gene Construction—Plasmids carrying the amino-terminal 604 amino acid residues of mouse IP_3R1, IP_3R2, and IP_3R3 ($T604_{m1}$, $T604_{m2}$, and $T604_{m3}$, respectively) were constructed as follows. The 1.8-kbp fragments of the three IP_3R genes were amplified with the PCR method from pBact-STneoB-C1, pBluescriptII-C2, and pBact-STneoB-C3 (5), with three pairs of primers, P1/P4, P2/P5, and P3/P4 (supplemental Table S1), respectively. The fragments were digested with NdeI and EcoRI and were subcloned into the modified pRSET-A (Invitrogen), in which the hexa-histidine (His_6) tag coding region was removed, to generate pRSET-$T604_{m1}$, pRSET-$T604_{m2}$, and pRSET-$T604_{m3}$, respectively. To express amino acid residues 224–604 of IP_3R2 and 225–604 of IP_3R3 (supplemental Fig. S1), plasmids were constructed as follows. The 1.1-kbp fragments were amplified from pBluescriptII-C2 and pBact-STneoB-C3 with pairs of primers, P6/P5, and P7/P4 (supplemental Table S1), respectively. The fragments were digested with NdeI and EcoRI and were subcloned into the His_6 tag-removed pRSET-A to generate pRSET-$(224–604)_{m2}$ and pRSET-$(225–604)_{m3}$, respectively. For the expression of residues 224–604 of mouse IP_3R1, pET-D-(1–223)/T604 (9) was used. For the expression of the His_6-tagged suppressor domain (residues 2–223) of mouse IP_3R1 (supplemental Fig. S1), pET23a-T7-IP_3R_{sup}-6His (7) was used. Plasmids carrying chimeric proteins, in which the suppressor domains were fused to the IP_3-binding core domain from different isoforms (supplemental Fig. S1), were constructed using the technique of splicing by overlap extension with PCR (10) and primers, P1, P3–5, P8, and P10–18 (supplemental Table S1). The combination of templates and primers used is summarized in supplemental Table S2. Mixtures of two DNA fragments separately produced in the first PCRs were used as templates for the second PCR (supplemental Table S2). The products of the second PCR were digested with NdeI and EcoRI and were subcloned into the His_6 tag-removed pRSET-A to generate pRSET-$(1–223)_{m2}$-$(224–604)_{m1}$, pRSET-$(1–224)_{m3}$-$(224–604)_{m1}$, pRSET-$(1–223)_{m1}$-$(224–604)_{m2}$, pRSET-$(1–224)_{m3}$-$(224–604)_{m2}$, pRSET-$(1–223)_{m1}$-$(225–604)_{m3}$, and pRSET-$(1–223)_{m2}$-$(225–604)_{m3}$, respectively.

Site-directed mutagenesis within the suppressor domain of $T604_{m3}$ or $(1–223)_{m1}$-$(225–604)_{m3}$ (supplemental Fig. S2) to engineer systematic chimeric proteins as summarized in supplemental Fig. S2 was performed with a Quick Change site-directed mutagenesis kit (Stratagene) and primers containing the appropriate substitution (M1–M13, supplemental Table S3). Multiple mutants were generated by sequential mutagenesis. Only sense primers used for the site-directed mutagenesis are shown in supplemental Table S3. Substitution of amino acid residues 61–122 of $T604_{m3}$ with amino acid residues 62–121 of $T604_{m1}$ was carried out using the technique of splicing by overlap extension with PCR (supplemental Table S2) and primers P3, P19, P20, and P21 (supplemental Table S1). The product of the second PCR was digested with NdeI, and the NdeI fragment (0.4 kbp) was replaced with the NdeI fragment (0.4 kbp) of pRSET-$T604_{m3}$. The nucleotide sequences of all of PCR prod-

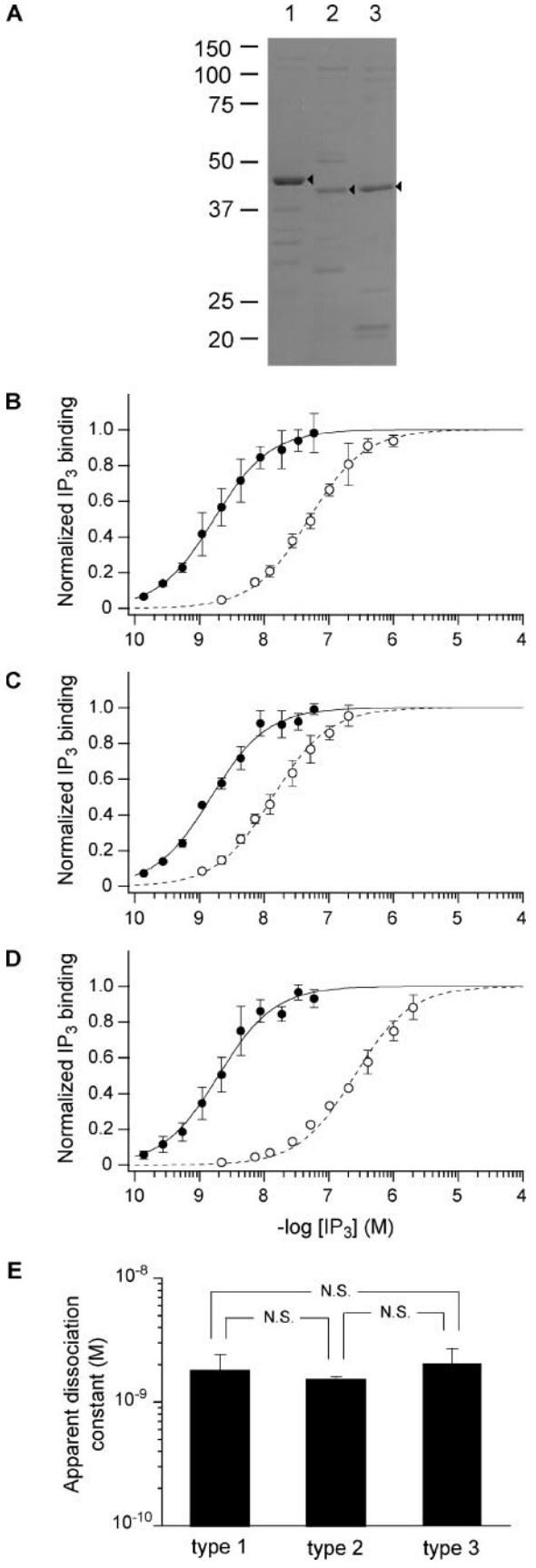

FIGURE 2. **Comparison of IP_3-binding affinity of the IP_3-binding core domain among the three IP_3R isoforms.** *A*, SDS-PAGE analysis. Purified proteins (0.75 μg) of $(224-604)_{m1}$ (*lane 1*), $(224-604)_{m2}$ (*lane 2*), and $(225-604)_{m3}$ (*lane 3*) were separated on 10% SDS-PAGE followed by Coomassie Brilliant Blue R-250 staining. *Arrowheads* indicate the proteins containing IP_3-binding core domains. Molecular size markers are shown on the *left* ($\times 10^3$). *B–D*, the relationship between normalized IP_3 binding and IP_3 concentrations applied. *Filled circles*: $(224-604)_{m1}$ (*B*), $(224-604)_{m2}$ (*C*), and $(225-604)_{m3}$ (*D*). The IP_3-binding activity of T604s shown in Fig. 1*B* is plotted as *open circles* (*B*, $T604_{m1}$; *C*, $T604_{m2}$; and *D*, $T604_{m3}$). *E*, comparison of the apparent dissociation constants of $(224-604)_{m1}$, $(224-604)_{m2}$, and $(225-604)_{m3}$. Averages of three independent measurements are shown. *Error bars* correspond to the standard deviation. Statistical analysis was performed using one-way analysis of variance followed by a post-hoc comparison using Dunn's multiple comparison procedure. *N.S.*, not significant.

ucts and site-directed mutants used in this study were confirmed by DNA sequencing with a 3130 Genetic analyzer (Applied Biosystems).

Expression and Purification of Recombinant Proteins—Recombinant proteins were expressed in *Escherichia coli* BL21-codonplus (Stratagene) as described previously (9). Protein purification was performed with a HiTrap heparin HP column (GE Healthcare) according to the method described previously (5). The His_6-tagged suppressor domain of mouse IP_3R1 (amino acid residues 2–223) was purified with a ProBond resin (Invitrogen) as described previously (5). Protein concentrations were determined with a protein assay kit (Bio-Rad) and bovine serum albumin as a standard.

IP_3 Binding Assay—An equilibrium IP_3 binding analysis of purified soluble proteins was performed as described previously (9), except for the reaction condition with a cytosol-like medium (110 mM KCl, 10 mM NaCl, 5 mM KH_2PO_4, and 50 mM Hepes-KOH, pH 7.4, at 4 °C). Purified protein (0.02–0.8 μg) was incubated with 0.14–8.68 nM $[^3H]IP_3$ (New England Nuclear/DuPont) and various concentrations of unlabeled IP_3 (Dojindo) in a binding buffer (cytosol-like medium containing 1 mM dithiothreitol and 0.5 mM EGTA). To avoid tracer depletion, the amount of the protein and the concentration of $[^3H]IP_3$ were adjusted for each experiment. Nonspecific binding was measured in the binding buffer without adding the protein. Nonlinear regression of IP_3 binding data with the Hill-Langmuir equation,

$$F = \frac{[IP_3]}{K_d + [IP_3]} \qquad \text{(Eq. 1)}$$

where F is the fraction of the recombinant protein that binds IP_3, $[IP_3]$ is the concentration of IP_3, and K_d is the apparent dissociation constant, was performed with Igor Pro (version 4.04, Wavematrics) software.

Modeling of the Suppressor Domain in IP_3R3—The structure of the IP_3R1 suppressor domain (residues 7–223) (7) was used for homology modeling of the suppressor domain structure of IP_3R3, residues 6–224. The sequence alignment between IP_3R1 and IP_3R3 was generated with ClustalW (11) and used for modeling with Modeller (12). Because the loop linking the two helices in the Arm sub-domain of IP_3R1 (residues 76–81) was not defined in the original structure, this portion of the suppressor domain was also modeled in the type-3 isoform. Thirty models were calculated and superimposed with Molmol (13) (root mean square deviation = 1.2 Å). Only the mean model is shown.

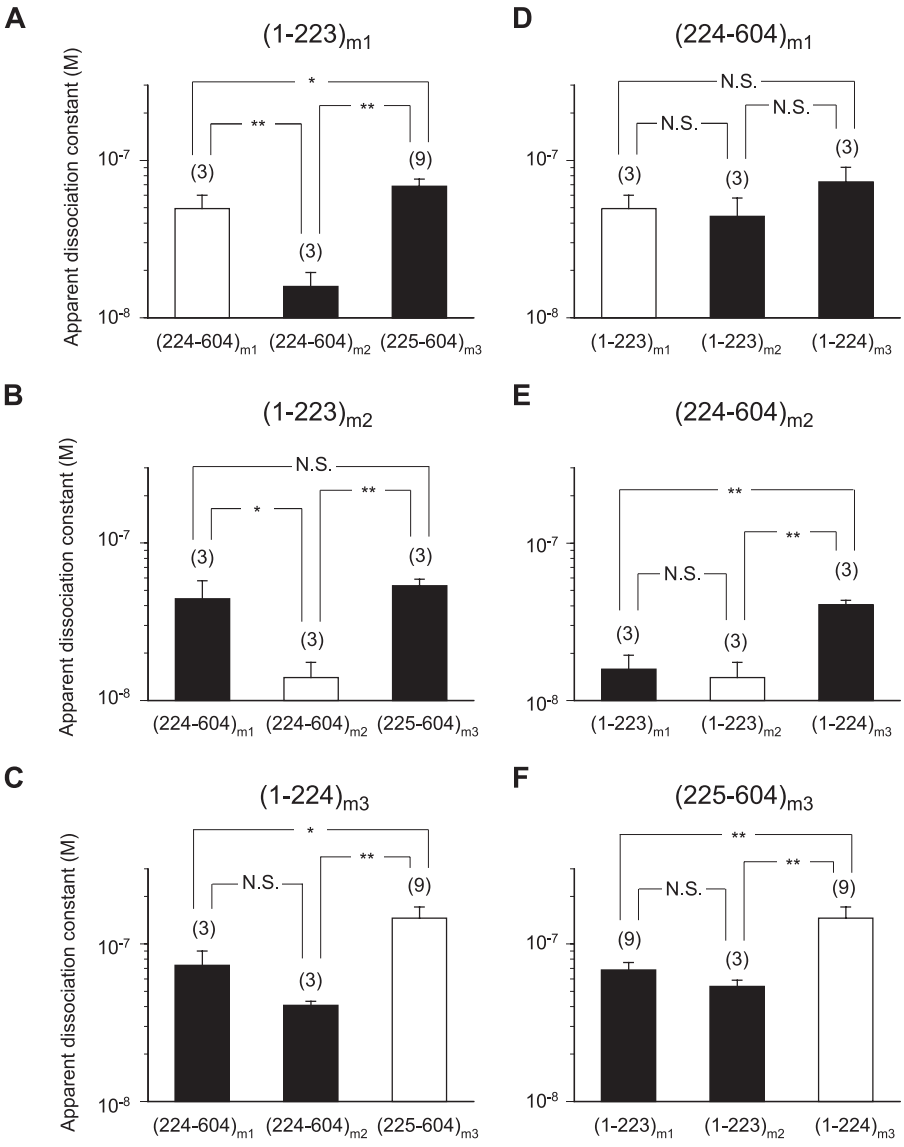

FIGURE 3. **Apparent dissociation constants of chimeric proteins in which the suppressor domain was fused to the IP_3-binding core domain from different isoforms.** *A–F*, average values of the apparent dissociation constant of the proteins with natural combinations of the suppressor domain and the IP_3-binding core domain (*open bar*) and of the chimeric proteins (*filled bar*) are shown. The number of measurements is shown in *parentheses*. *Error bars* correspond to the standard deviation. Statistical analyses were performed using one-way analysis of variance or Kruskal-Wallis test followed by a post-hoc comparison using Turkey-Kramer, Scheffe's F, or Dunn's multiple comparison procedure. *, $p < 0.05$; **, $p < 0.01$; *N.S.*, not significant.

RESULTS

Characterization of IP_3 Binding to the Amino-terminal 604 Residues of Three IP_3R Isoforms—Nontagged amino-terminal 604 amino acid residues of the three isoforms of mouse IP_3Rs, $T604_{m1}$, $T604_{m2}$, and $T604_{m3}$ (supplemental Fig. S1), were expressed in *E. coli* and were purified on a HiTrap heparin HP column. Recombinant T604 proteins showed an apparent molecular mass of ~65 kDa (Fig. 1*A*). We measured the IP_3-binding activity of these purified proteins using ^{3}H-labeled IP_3. Fig. 1*B* shows the relationship between the normalized amount of IP_3 bound to the purified proteins and the IP_3 concentration applied. Because the data of the three isoforms were well fitted with the Hill-Langmuir equation (see "Experimental Procedures") and each protein possesses a single IP_3-binding site, IP_3 binding to the purified amino-terminal 604 amino acid residues seemed to occur independently. The apparent dissociation constants of $T604_{m1}$, $T604_{m2}$, and $T604_{m3}$ were estimated to be 49.5 ± 10.5 nM ($n = 3$), 14.0 ± 3.5 nM ($n = 3$), and 163.0 ± 44.4 nM ($n = 9$) (mean ± S.D.), respectively. These values are well consistent with the intrinsic dissociation constants estimated from the analyses of homotetrameric IP_3R channels expressed in Sf9 cells under the same experimental condition (28.6 nM for IP_3R1, 5.9 nM for IP_3R2, and 294.0 nM for IP_3R3) (5) (Fig. 1*C*). These results suggest that the type-specific IP_3-binding affinity originates from the amino-terminal 604 amino acid residues of each IP_3R type.

Comparison of the IP_3-binding Affinity of the IP_3-binding Domain of Three Isoforms without the Suppressor Domain—The IP_3-binding domain of IP_3R1 is functionally divided into two parts: the amino-terminal suppressor domain and the carboxyl-terminal IP_3-binding core domain (6, 14). The IP_3-binding core domain has been defined as a minimum essential region for specific IP_3 binding, which resides within amino acid residues 226–578 of IP_3R1 (6). Because the amino acid residues 224–604 of mouse IP_3R1, designated as $(224–604)_{m1}$ (supplemental Fig. S1B), are expressed well in *E. coli* (9), we used it for the measurement of the IP_3-binding affinity of the IP_3-binding domain without the suppressor domain. Supplemental Fig. S1*A* shows portions of the amino acid sequence alignments among the three mouse IP_3R isoforms. To compare the unsuppressed IP_3-binding affinity among the three isoforms, we purified the bacterially expressed $(224–604)_{m1}$, residues 224–604 of mouse IP_3R2 ($(224–604)_{m2}$), and the residues 225–604 of mouse IP_3R3 ($(225–604)_{m3}$) (Fig. 2*A*). We found that all of the IP_3 binding data of these proteins were well fitted with the Hill-Langmuir equation (Equation 1) (Fig. 2, *B–D*) with statistically indistinguishable apparent dissociation constants, 1.78 ± 0.63 nM ($n = 3$) for $(224–604)_{m1}$, 1.51 ± 0.01 nM ($n = 3$) for $(224–604)_{m2}$, and 2.04 ± 0.65 nM ($n = 3$) for $(225–604)_{m3}$ (mean ± S.D.) (Fig. 2*E*). These results indicate that the presence of the amino-terminal 223, 223, and 224 amino acid residues of mouse IP_3R1, IP_3R2, and IP_3R3 results in the suppression of IP_3 binding by 27.8-fold (Fig. 2*B*), 9.3-fold (Fig. 2*C*), and 81.1-fold (Fig. 2*D*), respectively. Moreover, the isoform-specific IP_3-binding affinity of the

native IP_3Rs reflects the different degree of the suppression of IP_3 binding by the suppressor domain of each isoform.

Mechanism of IP_3 Binding Suppression—To assess the mechanism for the suppression, we investigated the effect of the addition of the bacterially expressed His_6-tagged amino acid residues 2–223 of mouse IP_3R1 ($H(2–223)_{m1}$) (supplemental Fig. S1) on the IP_3-binding activity of $(224–604)_{m1}$. As shown in supplemental Fig. S3 the addition of 100-fold excess (molar ratio) purified $H(2–223)_{m1}$ did not significantly alter the IP_3-binding affinity of $(224–604)_{m1}$. These results indicate that the suppression of IP_3 binding requires a covalent bond between the suppressor domain and the IP_3-binding core domain.

Functional Difference among the Suppressor Domains of the Three IP_3R Isoforms—We created six chimeric proteins composed of a suppressor domain fused with an IP_3-binding core domain from different isoforms (supplemental Fig. S1*B*) to analyze the mechanism underlying the generation of isoform-specific IP_3-binding affinity. All of the equilibrium IP_3 binding data obtained for these chimeric proteins showed good fits with the Hill-Langmuir equation (Equation 1, data not shown) with apparent dissociation constants of 44.2 ± 13.4 nM ($n = 3$) for $(1–223)_{m2}$-$(224–604)_{m1}$, 73.0 ± 17.3 nM ($n = 3$) for $(1–224)_{m3}$-$(224–604)_{m1}$, 15.8 ± 3.6 nM ($n = 3$) for $(1–223)_{m1}$-$(224–604)_{m2}$, 40.7 ± 2.6 nM ($n = 3$) for $(1–224)_{m3}$-$(224–604)_{m2}$, 65.9 ± 7.4 nM ($n = 9$) for $(1–223)_{m1}$-$(225–604)_{m3}$, and 53.7 ± 5.2 nM ($n = 3$) for $(1–223)_{m2}$-$(225–604)_{m3}$ (mean ± S.D.). The results of the statistical analyses of these data are shown in Fig. 3. All of the chimeric proteins showed >10-fold lower IP_3-binding affinity (Fig. 3, *A–C*) compared with the proteins that do not possess the suppressor domain ($K_d \approx 2$ nM) (Fig. 2). The artificial chimeric proteins, however, revealed apparent dissociation constants that significantly differed from those of the proteins composed of the native combination of the suppressor domain and the IP_3-binding core domain (Fig. 3, *A–C*). This suggests that the suppressor domain alone is not a prime determinant of the affinity for IP_3. When we compare the same data in respect of the IP_3-binding core domain (Fig. 3, *D–F*), the different character of the IP_3-binding core domain of the three isoforms became obvious. The IP_3-binding core domain of the type-1 isoform exhibited an almost identical IP_3-binding affinity despite the type of the suppressor domain connected (Fig. 3*D*). The type-2 IP_3-binding core domain showed indistinguishable affinity for IP_3 when it was fused with the type-1 and type-2 suppressor domains, but the chimeric protein with the type-3 suppressor domain showed an affinity ~3-fold lower compared with the native combination of the type-2 isoform (Fig. 3*E*). The IP_3-binding core domain of the type-3 isoform strictly required the type-3 suppressor domain to generate its native IP_3-binding affinity (Fig. 3*F*). These results indicate that: 1) the isoform-specific IP_3-binding affinity is predominantly determined by the IP_3-binding core domain rather than the suppressor domain; 2) the suppressor domains of the type-1 isoform and type-2 isoform are mutually interchangeable for both the IP_3-binding core domains of IP_3R1 and IP_3R2 to generate their native IP_3-binding affinity; and 3) the type-3-specific site(s) in the suppressor domain may be critical for the proper suppression of the IP_3-binding core domain of IP_3R3.

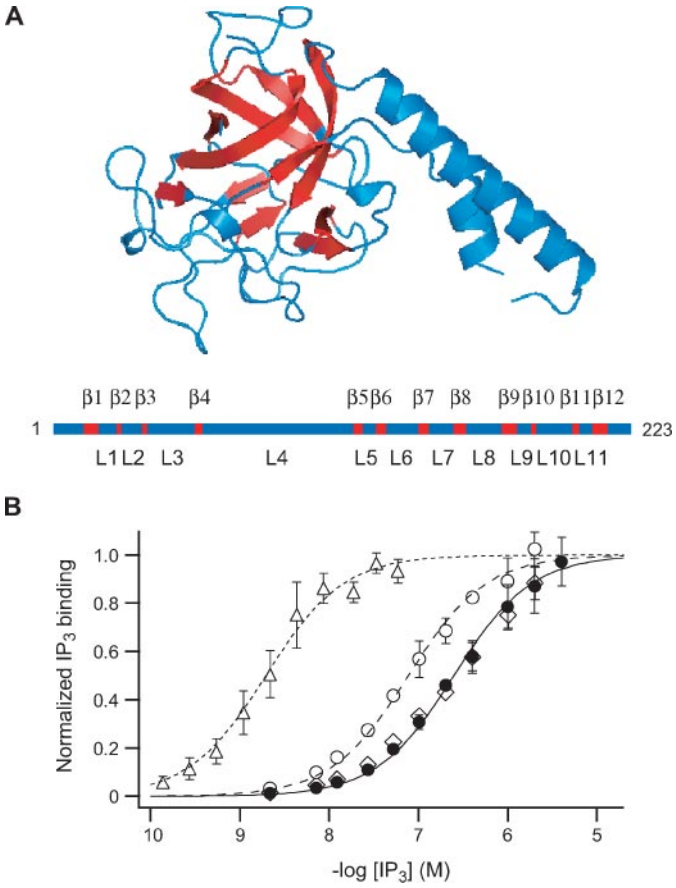

FIGURE 4. **IP_3-binding activity of a mutant protein in which all of type-3-specific amino acid residues within the β-strands of the suppressor domain were replaced with those appearing in IP_3R1.** *A*, three-dimensional structure of the suppressor domain of mouse IP_3R1. Twelve β-strands and eleven loop regions are shown in *red* and *blue*, respectively. Boundaries of the β-strands and loop regions are determined as described previously (7). *B*, equilibrium IP_3-binding activity of $(\beta1,\beta4,\beta8,\beta9,\beta12)_{m1}/T604_{m3}$ ($n = 3$, *closed circle*), $T604_{m3}$ (*open diamond*), $(1–223)_{m1}$-$(225–604)_{m3}$ (*open circle*), and $(225–604)_{m3}$ (*open triangle*) is shown. *Error bars* correspond to the standard deviation.

Critical Loop Regions in the Suppressor Domain for the Suppression of IP_3R3—To elucidate the structural basis for the suppression of the type-3 isoform, we created a series of mutated proteins based on the amino acid sequence difference between IP_3R1 and IP_3R3 and on the three-dimensional structure of the suppressor domain of IP_3R1 (supplemental Fig. S2). The suppressor domain forms a hammer-like structure with the head subdomain and the arm subdomain (7). The head subdomain consists of two single-turn α-helices and 12 β-strands, which form a β-trefoil fold (7). The arm subdomain is made of a helix-turn-helix structure, which is inserted between the fourth and fifth β-strands of the head subdomain (7). We hypothesized that the critical regions for the suppression of the type-3 isoform are located within the 11 loop segments that connect β-strands (Figs. 4*A* and S2), because in the case of β-trefoil fold architecture most of the surface properties are dictated by the residues from the loop segment, rather than the residues comprising the barrel and the triangular array of the core structure (15). To evaluate this hypothesis, we first constructed a mutant protein in which all of the non-conserved amino acid residues within the β-strand regions of $T604_{m3}$ were substituted with

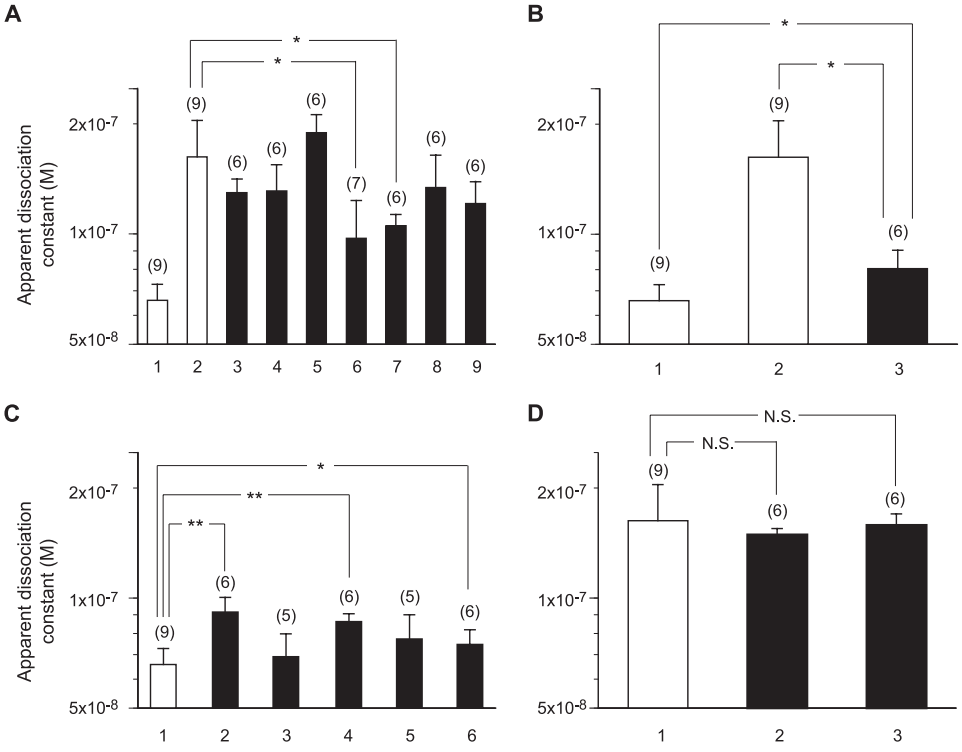

FIGURE 5. **Identification of the loop regions critical for the suppression of IP_3 binding to the type-3 IP_3-binding core domain.** *A*, apparent dissociation constants of $(1–223)_{m1}$-$(225–604)_{m3}$ (*lane 1*), $T604_{m3}$ (*lane 2*), $L1_{m1}/T604_{m3}$ (*lane 3*), $L3_{m1}/T604_{m3}$ (*lane 4*), $L4_{m1}/T604_{m3}$ (*lane 5*), $L5_{m1}/T604_{m3}$ (*lane 6*), $L7_{m1}/T604_{m3}$ (*lane 7*), $L8_{m1}/T604_{m3}$ (*lane 8*), and $L10_{m1}/T604_{m3}$ (*lane 9*). *B*, apparent dissociation constants of $(1–223)_{m1}$-$(225–604)_{m3}$ (*lane 1*), $T604_{m3}$ (*lane 2*), and $(L5,L7)_{m1}/T604_{m3}$ (*lane 3*). *C*, apparent dissociation constants of $(1–223)_{m1}$-$(225–604)_{m3}$ (*lane 1*), $(L1,L5,L7)_{m1}/T604_{m3}$ (*lane 2*), $(L3,L5,L7)_{m1}/T604_{m3}$ (*lane 3*), $(L4,L5,L7)_{m1}/T604_{m3}$ (*lane 4*), $(L5,L7,L8)_{m1}/T604_{m3}$ (*lane 5*), and $(L5,L7,L10)_{m1}/T604_{m3}$ (*lane 6*). *D*, apparent dissociation constants of $T604_{m3}$ (*lane 1*), $(L3,L5,L7)_{m3}/(1–223)_{m1}$-$(225–604)_{m3}$ (*lane 2*), and $(L5,L7,L8)_{m3}/(1–223)_{m1}$-$(225–604)_{m3}$ (*lane 3*). The number of measurements is shown in parentheses. *, $p < 0.05$; **, $p < 0.01$; *N.S.*, not significant (Student's *t* test). The mutants used in this study are summarized in supplemental Fig. S2.

residues appearing in IP_3R1 (supplemental Fig. S2). Non-conserved residues are located within the first, fourth, eighth, ninth, and twelfth β-strand regions ($\beta1$, $\beta4$, $\beta8$, $\beta9$, and $\beta12$, respectively, supplemental Fig. S2) (7). The mutant protein, $(\beta1,\beta4,\beta8,\beta9,\beta12)_{m1}/T604_{m3}$, exhibited an apparent dissociation constant of 254.0 ± 48.5 nM ($n = 3$), which was indistinguishable from that of $T604_{m3}$ (163.0 ± 44.4 nM) ($n = 9$) (Fig. 4*B*). These results indicate that the critical sites for type-3-specific suppression are located within the loop regions, but not within the β-strand regions, of the suppressor domain. Type-3-specific amino acid sequences are located within the first, third, fourth, fifth, seventh, eighth, and tenth loop regions (L1, L3, L4, L5, L7, L8, and L10, respectively, supplemental Fig. S2) (7).

To identify critical sites within the suppressor domain for the suppression of IP_3 binding to the type-3 IP_3-binding core domain, we created seven mutant proteins in which the amino acid sequences of individual type-3-specific loop regions, L1, L3, L4, L5, L7, L8, and L10, were substituted with residues appearing in IP_3R1 (supplemental Fig. S2). We found that both $L5_{m1}/T604_{m3}$ (97.4 ± 26.2 nM, $n = 7$) and $L7_{m1}/T604_{m3}$ (105.0 ± 7.8 nM, $n = 6$) exhibited an apparent dissociation constant, which was significantly different from that of $T604_{m3}$ (Fig. 5*A*). These results showed that both L5 and L7 are required for the suppression of IP_3 binding to the IP_3-binding core domain of IP_3R3. We then constructed a mutant protein in which type-3-specific amino acid residues within both L5 and L7 in $T604_{m3}$ were simultaneously changed to the residues that appear in IP_3R1 (supplemental Fig. S2). This mutant protein, $(L5,L7)_{m1}/T604_{m3}$, exhibited an apparent dissociation constant (80.6 ± 9.9 nM, $n = 6$) that was lower than those of $L5_{m1}/T604_{m3}$ and $L7_{m1}/T604_{m3}$ (Fig. 5*B*), but the effect of the simultaneous replacement was not statistically significant when compared with the effects of the single loop replacements. The apparent dissociation constant of $(L5,L7)_{m1}/T604_{m3}$ is significantly different from that of $(1–223)_{m1}$-$(225–604)_{m3}$ (Fig. 5*B*). We then created five mutant proteins, $(L1,L5,L7)_{m1}/T604_{m3}$, $(L3,L5,L7)_{m1}/T604_{m3}$, $(L4,L5,L7)_{m1}/T604_{m3}$, $(L5,L7,L8)_{m1}/T604_{m3}$, and $(L5,L7,L10)_{m1}/T604_{m3}$, in which the type-3-specific amino acid residues in three loop regions, including L5 and L7, were substituted with residues appearing in IP_3R1 (supplemental Fig. S2). Among these mutants, $(L3,L5,L7)_{m1}/T604_{m3}$ and $(L5,L7,L8)_{m1}/T604_{m3}$ exhibited an apparent dissociation constant (69.2 ± 10.6 nM ($n = 5$) and 77.4 ± 12.7 nM ($n = 5$), respectively) that was not different significantly from that of $(1–223)_{m1}$-$(225–604)_{m3}$ ($p = 0.525$ and 0.066, respectively, Fig. 5*C*). To confirm these results, we created mutant proteins in which all of the type-1-specific amino acid residues within L3, L5, and L7 in $(1–223)_{m1}$-$(225–604)_{m3}$ or within L5, L7, and L8 in $(1–223)_{m1}$-$(225–604)_{m3}$ were substituted with residues appearing in IP_3R3 (supplemental Fig. S2). The mutants, $(L3,L5,L7)_{m3}/(1–223)_{m1}$-$(225–604)_{m3}$ and $(L5,L7,L8)_{m3}/(1–223)_{m1}$-$(225–604)_{m3}$, exhibited an apparent dissociation constant of 149.0 ± 5.8 nM ($n = 6$) and 158.0 ± 11.5 nM ($n = 6$), respectively, both of which are indistinguishable from that of $T604_{m3}$ (Fig. 5*D*). We therefore concluded that L5 and L7 plus either L3 or L8 in the suppressor domain are essential and sufficient for the generation of type-3-specific IP_3-binding affinity of the IP_3-binding core domain of IP_3R3.

Type-3-specific Amino Acid Residues Critical for the Suppression of IP_3 Binding to the Type-3 IP_3-binding Core Domain—Fig. 6 shows amino acid sequence alignments of L3, L5, L7, and L8 of the suppressor domain of the three IP_3R types. The amino acid residues specific for IP_3R3, but not for IP_3R1, are Glu-39, Ala-41, and Asp-46 in L3, Met-127 in L5, Ala-154, Thr-155, and Leu-162 in L7, and Trp-168, Asn-173, Asn-176, and Val-179 in L8 (Fig. 6). All of the amino acid residues except Leu-162 are located at the surface of the suppressor domain of IP_3R3 (Fig. 7).

```
Loop3
IP3R1  39  VQPEAGDLNNPPKKFRDCL  57
IP3R2  39  VHPEAGDLANPPKKFRDCL  57
IP3R3  38  VEPAAGDLDNPPKKFRDCL  56

Loop5
IP3R1 126  LKSNK  130
IP3R2 126  IKSNK  130
IP3R3 127  MKSNK  129

Loop7
IP3R1 152  DEAGNEGSWF  161
IP3R2 152  DAAGNEGSWF  161
IP3R3 153  DATGNEGSWL  162

Loop8
IP3R1 167  YKLRSIGDSVVIGD  180
IP3R2 167  WKLRSEGDNIVVGD  180
IP3R3 168  WKLRSNGDNVVVGD  181
```

FIGURE 6. **Amino acid sequence alignments of the third, fifth, seventh, and eighth loop regions of the suppressor domain.** Amino acid residues identified to be critical for the suppression of IP_3 binding to type-3-IP_3-binding core domain are shown in *red*. Type-2-unique residues are shown in *blue*.

DISCUSSION

The IP_3 sensitivity of the intracellular Ca^{2+} stores seems to be heterogenous within the cytosol, and spatially restricted Ca^{2+} releases, such as Ca^{2+} puffs, have frequently been observed in various cell types (16, 17). Multiple intracellular Ca^{2+} stores with variable IP_3 sensitivities in single cells may contribute to the generation of the complex spatiotemporal patterns of intracellular Ca^{2+} dynamics (18–21). We have previously reported that three isoforms of the IP_3R have different IP_3-binding affinities and cooperativities (5). A non-cooperative IP_3 binding model did not fit the equilibrium IP_3 binding data obtained from tetrameric IP_3R2 or IP_3R3 complexes expressed in Sf9 cells (5), indicating that the IP_3-binding affinity of vacant subunits within single tetrameric complexes changes depending on the number of occupied subunits within a homotetrameric complex composed of IP_3R2 or IP_3R3. The intrinsic IP_3-binding affinities, that is the IP_3-binding affinities of four vacant subunits within single non-liganded homotetrameric complexes, have been estimated to be $3.5 \times 10^7\ M^{-1}$ for IP_3R1, $1.7 \times 10^8\ M^{-1}$ for IP_3R2, and $3.4 \times 10^6\ M^{-1}$ for IP_3R3 (5). In the present study, we analyzed the molecular basis of the isoform-specific intrinsic IP_3-binding affinity of IP_3R. The amino-terminal 604 amino acid residues of the three isoforms exhibited almost the same IP_3-binding affinities with the intrinsic IP_3-binding affinities estimated from full-length IP_3Rs expressed in Sf9 cells (Fig. 1). These results indicate that the intrinsic IP_3-binding affinity of homotetrameric IP_3R channels is predominantly determined by the amino-terminal 604 amino acid residues of each subunit. The amino-terminal 225 residues have been known to reduce the IP_3-binding affinity of the IP_3-binding core domain of IP_3R1 by >10-fold (6), and the deletion of the amino-terminal 225 residues has been reported to enhance the IP_3-binding activity of IP_3R3 (22); however, the effect of the suppressor domain on the affinity of the IP_3-binding core domain has never been quantitatively characterized for type-2 and type-3 isoforms. We measured the IP_3-binding affinity of residues 224–604 of IP_3R2 and residues 225–604 of IP_3R3 and found that both proteins showed an IP_3-binding affinity higher than those obtained for residues 1–604 of IP_3R2 and IP_3R3 by 9.3- and 81.1-fold, respectively (Fig. 2). Interestingly, in the absence of the suppressor domain, all three isoforms exhibit a nearly identical IP_3-binding affinity (Fig. 2). Because Bultynck *et al.* (23) has shown that the suppressor domain of IP_3R1 (residues 1–225) can physically interact with the IP_3-binding core domain of IP_3R1 (residues 226–604), the interdomain interaction may cause changes in the IP_3-binding affinity of the IP_3-binding core domain. The amino-terminal 604 residues of three IP_3R types bind IP_3 in a non-cooperative manner (Fig. 1*B*), indicating that the suppression of IP_3 binding occurs independently in each molecule. Because the addition of a 100-fold excess of the suppressor domain did not significantly alter the IP_3-binding affinity of the IP_3-binding core domain (supplemental Fig. S3), the suppressor domain is not effective for separating molecules. We therefore suspect that the suppression of IP_3 binding is an intramolecular event that requires a covalent bond between the suppressor domain and the IP_3-binding core domain. The present results suggest that 1) the isoform-specific IP_3-binding affinity originates from the intramolecular suppression of IP_3 binding, but not from the difference in the intrinsic IP_3-binding affinity of the IP_3-binding core domain, and 2) the nature of the interaction between the suppressor domain and the IP_3-binding core domain is different among the three isoforms, thereby resulting in their different IP_3-binding affinities. In other words, the IP_3-binding affinity of IP_3Rs is generated by the precisely controlled attenuation of IP_3-binding affinity caused by the intramolecular interaction between the suppressor domain and the IP_3-binding core domain, and the IP_3-binding affinity is a tunable parameter rather than a stable constant.

Molecular Basis of the Type-specific Suppression of IP_3 Binding—To test domain compatibility among the three IP_3R types, we have engineered chimeric proteins in which the amino-terminal suppressor domain was fused to the IP_3-binding core domain from different isoforms and found that the suppressor domain is not a prime determinant of the IP_3-binding affinity (Fig. 3, *A–C*). The IP_3-binding core domain of IP_3R1 showed almost the same apparent dissociation constants regardless of the type of the suppressor domain connected (Fig. 3*D*). The IP_3-binding core domain of IP_3R2 did not discriminate the suppressor domain from IP_3R1 and IP_3R2, but the suppressor domain from IP_3R3 failed to produce the native IP_3-binding affinity of IP_3R2 (Fig. 3*E*). The IP_3-binding core domain of IP_3R3 strictly required the suppressor domain from the same isoform to produce its native IP_3-binding affinity (Fig. 3*F*). These results indicate that 1) conserved amino acid residues in the suppressor domain of IP_3R1 and IP_3R2 are involved in the interaction with the type-1 and type-2 IP_3-binding core do-

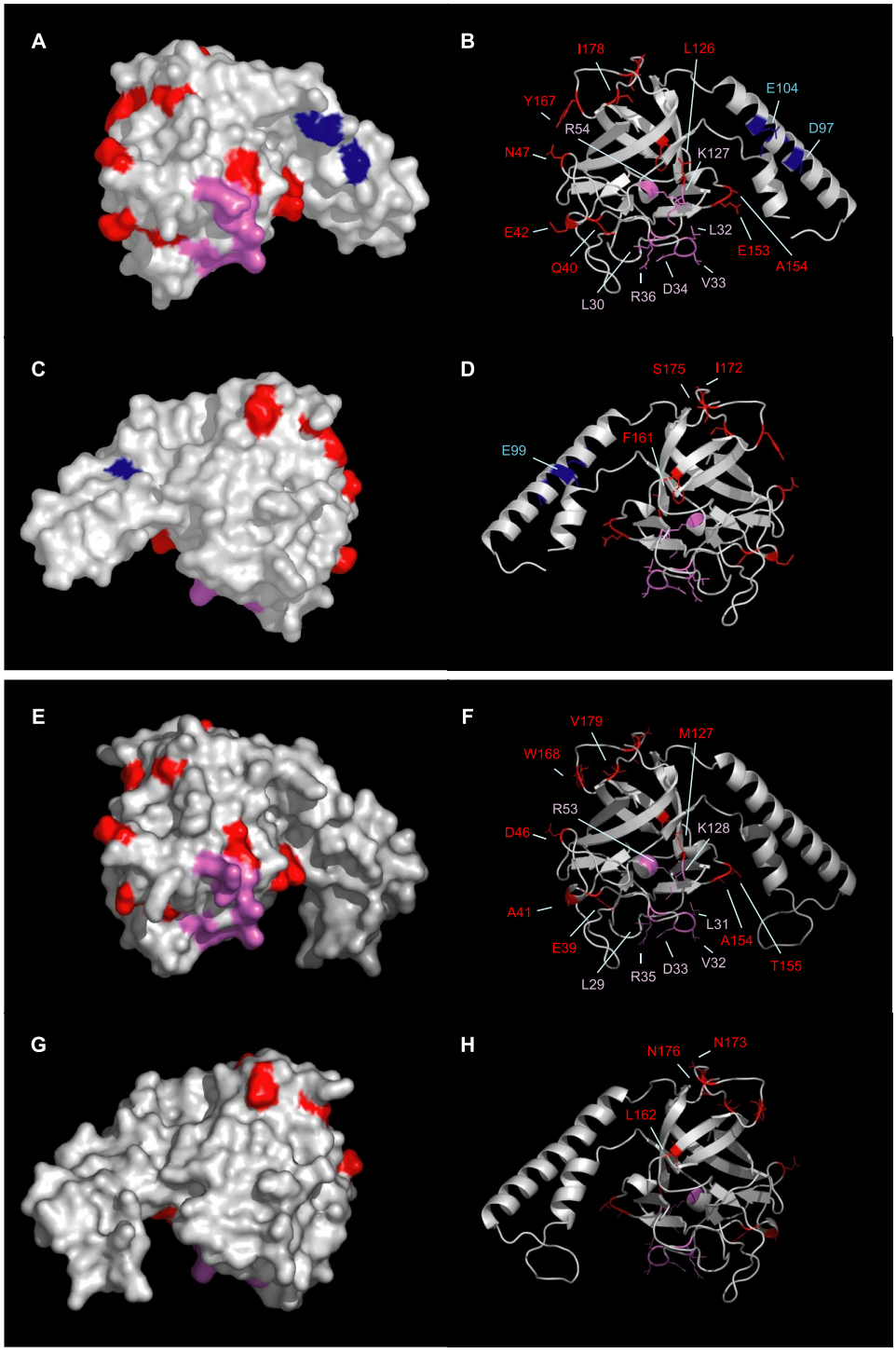

FIGURE 7. **Surface and ribbon diagram representations of critical sites for the IP_3 binding suppression.** Surface (*A* and *C*) and ribbon diagram (*B* and *D*) representations of the suppressor domain of mouse IP_3R1 and surface (*E* and *G*) and ribbon diagram (*F* and *H*) representations of the suppressor domain of mouse IP_3R3 are shown. The amino acid residues critical for the type-specific suppression are depicted in *red*. The conserved amino acid residues essential for the IP_3 binding suppression (7) are labeled in *pink*. Amino acid residues in *blue* are involved in the determination of the IP_3-binding affinity of IP_3R1 (7). *C*, view in *A* rotated by 180°. *D*, view in *B* rotated by 180°. *G*, view in *E* rotated by 180°. *H*, view in *F* rotated by 180°.

Identification of Amino Acid Residues Critical for the Type-3-specific IP_3-binding Affinity—Systematic mutagenesis analyses (Figs. 4 and 5) showed that at least L5 and L7 in the suppressor domain are essential for the generation of the type-3-specific IP_3-binding affinity. Interestingly, $(L3,L5,L7)_{m1}/T604_{m3}$ and $(L5,L7,L8)_{m1}/T604_{m3}$ exhibited an apparent dissociation constant indistinguishable from that of $(1–223)_{m1}$-$(225–604)_{m3}$ (Fig. 5*C*) and $(L3,L5,L7)_{m3}/(1–223)_{m1}$-$(225–604)_{m3}$ and $(L5,L7,L8)_{m3}/(1–223)_{m1}$-$(225–604)_{m3}$ exhibited an apparent dissociation constant indistinguishable from that of $T604_{m3}$ (Fig. 5*D*). These results suggest that, in addition to L5 and L7, either L3 or L8 is required for the generation of the native IP_3-binding affinity of IP_3R3. This interpretation seems to be supported by the results shown in Fig. 5*A*. The replacement of either L5 or L7 from $T604_{m3}$ resulted in a significant enhancement of the IP_3-binding affinity, whereas, single replacement of either L3 or L8 did not result in a significant alteration of the IP_3-binding affinity (Fig. 5*A*). The position of L5 and L7 are relatively close on the suppressor domain and the three type-3-specific amino acid residues, Met-127, Ala-154, and Thr-155, within these regions are nearby the previously identified conserved residues essential for the suppression of IP_3 binding to IP_3R1 (Fig. 7). L3 is located on the same side of L5 and L7 on the suppressor domain, whereas L8 is placed on the opposite side (Fig. 7). These results predict a dynamic nature of the intramolecular interaction for the suppression of IP_3 binding. More specifically, there are at least two different conformational states of the complex comprising the suppressor domain and IP_3-binding core domain with both states contributing toward the suppression of IP_3 binding. One possible interpretation is that one of the complexes employs an interface formed by L3, L5, and L7 on the suppressor domain, whereas the other uses an interface formed by L5, L7, and L8. The amino acid sequences of these critical loops might also indirectly affect the structure of the interface

mains, and 2) type-3-specific amino acid residues are strictly required for the proper interaction with the type-3 IP_3-binding core domain. Type-3-specific residues may also interfere in the proper interaction with the type-2 IP_3-binding core domain.

between the suppressor domain and the IP_3-binding domain. According to the prediction, the essential amino acid residues for the generation of the type-3 receptor-specific IP_3-binding affinity are Glu-39, Ala-41, Asp-46, Met-127, Ala-154, Thr-155, Leu-162, Trp-168, Asn-173, Asn-176, and Val-179 (Figs. 6 and 7). Szlufcik *et al.* showed that the deletion of amino acid residues 76–86 of IP_3R1 or the replacement of these residues by residues 75–86 of IP_3R3 resulted in an increase in IP_3 binding and the sensitivity of IP_3-induced Ca^{2+} release (22). In our experiments, the replacement of L4, which includes residues 76–86 of IP_3R1 or residues 75–86 of IP_3R3, did not induce a significant change in the apparent dissociation constant of $T604_{m3}$ (Fig. 5*A*). Because Szlefcik *et al.* (22) measured the amount of $[^3H]IP_3$ bound to crude membrane fractions prepared from cell lines with different expression levels of recombinant receptors, it is not clear whether the mutations on residues 76–86 significantly affected the IP_3-binding affinity of the actual receptor proteins. Because our results reported here are mainly based on an analysis of the IP_3-binding domain fragments expressed in bacteria, the critical sites for determining isoform-specific IP_3-binding affinity in full-length receptor proteins should be confirmed. Identification of the interface between the suppressor domain and the IP_3-binding core domain by x-ray or NMR analyses should help our better understanding of the nature of the molecular interaction between these two domains.

A Possible Mechanism for the Suppression of IP_3 Binding—Addition of 100-fold excess of the type-1 suppressor domain did not result in a significant reduction of the IP_3-binding affinity of the type-1 IP_3-binding core domain (supplemental Fig. S3). This result indicates that the suppression of IP_3 binding is not a simple competitive inhibition of IP_3 binding to the IP_3-binding core domain by the suppressor domain. Recently, we have measured the reaction kinetics of the fluorescence resonance energy transfer of the IP_3 sensor protein upon the IP_3 binding (24). The IP_3 sensor protein, designated IRIS, is composed of the type-1 IP_3-binding core domain fused to two fluorescent proteins, enhanced cyan fluorescent protein and Venus. Analysis of the reaction kinetics of IRIS shows that there are at least two conformational states of the IP_3-binding core domain in the absence of IP_3 and that IP_3 binding fixes the conformation of the IP_3-binding core domain to one state (24). This reaction model is consistent with the result of the NMR studies, which suggests a dynamic equilibrium exists between two or more conformations in the apo state of the IP_3-binding core domain (25). According to this model, not only the rate constants for ligand-association and dissociation but also the rate constants for conformational changes of the receptor protein determine the equilibrium dissociation constant between the receptor and ligand. Evaluation of the effect of the suppressor domain on the rate of ligand binding and the rate of conformational changes of the IP_3-binding domain should help us to understand the mechanism of the IP_3 binding suppression.

Functional Significance of the Intramolecular Turning of IP_3-binding Affinity—What is the functional significance of the intramolecular attenuation of the intrinsic IP_3-binding affinity of IP_3Rs except for the generation of the isoform-specific IP_3-binding affinity? We have previously shown that the IP_3 binding to the tetrameric complex of IP_3R2 or IP_3R3 is not a random process, and the occupation of the IP_3-binding site changes the IP_3-binding affinity of vacant sites on the neighboring subunits (5). During the sequential binding of four IP_3 molecules to single tetrameric complexes of IP_3R2 and IP_3R3, the dissociation constants of vacant sites are estimated to be changed to 5.8×10^{-9} M (0 IP_3 molecule/tetramer), 3.7×10^{-8} M (1 IP_3 molecule/tetramer), 1.3×10^{-6} M (2 IP_3 molecules/tetramer), and 3.4×10^{-7} M (3 IP_3 molecules/tetramer) for IP_3R2 and to 2.9×10^{-7} M (0 IP_3 molecule/tetramer), 7.0×10^{-7} M (1 IP_3 molecule/tetramer), 8.2×10^{-7} M (2 IP_3 molecules/tetramer), and 2.8×10^{-6} M (3 IP_3 molecules/tetramer) for IP_3R3, respectively (5). These flexible changes of IP_3-binding affinity may be generated from the molecular interaction between occupied subunits and vacant subunits within a single tetrameric channel complex through the suppressor domain of vacant subunits. We have also pointed out that the suppressor domain is a focal point for the interaction with various modulatory proteins, including calmodulin, CaBP1, and RACK1 (7). These proteins may have some potential for the modulation of the IP_3-binding affinity of IP_3Rs by changing the degree of the suppression of IP_3 binding. Our recent analysis of cytosolic IP_3 dynamics in single living cells suggest that IP_3 sensitivity of the intracellular Ca^{2+} stores continuously change during Ca^{2+} oscillations (24). The unique ligand binding machinery, composed of the suppressor domain and the IP_3-binding core domain of IP_3Rs, may account for the generation of the dynamic change of the sensitivity of the receptor for IP_3 in living cells.

Acknowledgments—We thank Dr. Haruka Yamazaki for technical help and Drs. Anita Aperia, Per Uhlen, and Fumio Yoshikawa for fruitful discussions.

REFERENCES

1. Furuichi, T., Kohda, K., Miyawaki, A., and Mikoshiba, K. (1994) *Curr. Opin. Neurobiol.* **4,** 294–303
2. Monkawa, T., Miyawaki, A., Sugiyama, T., Yoneshima, H., Yamamoto-Hino, M., Furuichi, T., Saruta, T., Hasegawa, M., and Mikoshiba, K. (1995) *J. Biol. Chem.* **270,** 14700–14704
3. Newton, C. L., Mignery, G. A., and Sudhof, T. C. (1994) *J. Biol. Chem.* **269,** 28613–28619
4. Nerou, E. P., Riley, A. M., Potter, B. V., and Taylor, C. W. (2001) *Biochem. J.* **355,** 59–69
5. Iwai, M., Tateishi, Y., Hattori, M., Mizutani, A., Nakamura, T., Futatsugi, A., Inoue, T., Furuichi, T., Michikawa, T., and Mikoshiba, K. (2005) *J. Biol. Chem.* **280,** 10305–10317
6. Yoshikawa, F., Morita, M., Monkawa, T., Michikawa, T., Furuichi, T., and Mikoshiba, K. (1996) *J. Biol. Chem.* **271,** 18277–18284
7. Bosanac, I., Yamazaki, H., Matsu-ura, T., Michikawa, T., Mikoshiba, K., and Ikura, M. (2005) *Mol. Cell* **17,** 193–203
8. Bosanac, I., Alattia, J. R., Mal, T. K., Chan, J., Talarico, S., Tong, F. K., Tong, K. I., Yoshikawa, F., Furuichi, T., Iwai, M., Michikawa, T., Mikoshiba, K., and Ikura, M. (2002) *Nature* **420,** 696–700
9. Yoshikawa, F., Uchiyama, T., Iwasaki, H., Tomomori-Satoh, C., Tanaka, T., Furuichi, T., and Mikoshiba, K. (1999) *Biochem. Biophys. Res. Commun.* **257,** 792–797
10. Horton, R. M., Hunt, H. D., Ho, S. N., Pullen, J. K., and Pease, L. R. (1989) *Gene* (*Amst.*) **77,** 61–68
11. Thompson, J. D., Higgins, D. G., and Gibson, T. J. (1994) *Nucleic Acids Res.* **22,** 4673–4680
12. Sali, A., and Blundell, T. L. (1993) *J. Mol. Biol.* **234,** 779–815

13. Koradi, R., Billeter, M., and Wuthrich, K. (1996) *J. Mol. Graph.* **14,** 51–55
14. Yoshikawa, F., Iwasaki, H., Michikawa, T., Furuichi, T., and Mikoshiba, K. (1999) *J. Biol. Chem.* **274,** 328–334
15. Murzin, A. G., Lesk, A. M., and Chothia, C. (1992) *J. Mol. Biol.* **223,** 531–543
16. Bootman, M. D., and Berridge, M. J. (1995) *Cell* **83,** 675–678
17. Parker, I., Choi, J., and Yao, Y. (1996) *Cell Calcium* **20,** 105–121
18. Bootman, M. D., Berridge, M. J., and Taylor, C. W. (1992) *J. Physiol.* **450,** 163–178
19. Taylor, C. W. (1992) *Adv. Second Messenger Phosphoprotein Res.* **26,** 109–142
20. Berridge, M. J., and Dupont, G. (1994) *Curr. Opin. Cell Biol.* **6,** 267–274
21. Marchant, J., Callamaras, N., and Parker, I. (1999) *EMBO J.* **18,** 5285–5299
22. Szlufcik, K., Bultynck, G., Callewaert, G., Missiaen, L., Parys, J. B., and De Smedt, H. (2006) *Cell Calcium* **39,** 325–336
23. Bultynck, G., Szlufcik, K., Kasri, N. N., Assefa, Z., Callewaert, G., Missiaen, L., Parys, J. B., and De Smedt, H. (2004) *Biochem. J.* **381,** 87–96
24. Matsu-ura, T., Michikawa, T., Inoue, T., Miyawaki, A., Yoshida, M., and Mikoshiba, K. (2006) *J. Cell Biol.* **173,** 755–765
25. Bosanac, I., Michikawa, T., Mikoshiba, K., and Ikura, M. (2004) *Biochim. Biophys. Acta* **1742,** 89–102